Application of Liutex and Entropy Production to Analyze the Influence of Vortex Rope in the Francis-99 Turbine Draft Tube

Cong Trieu TRAN*, Duc Cuong PHAM

Abstract: The vortex structures in a draft tube of a Francis turbine are confused, primarily when cavitation occurs, which may induce severe vibration and noise. Understanding this vortex's periodical precession and investigating the vortex rope influence in the draft tube cone is required for stable operation at off-design conditions. This study captured the cavitating flow with high accuracy by utilizing the SST turbulence and ZGB cavitation models. The Omega and Liutex methods are employed and compared with the traditional Q - criterion to determine the vortex rope behavior in the Francis-99 turbine draft tube. The result showed that the Liutex/Rortex method is advantageous over the Q - criterion for representing the vortex rope structure. The Liutex method can effectively remove the boundary layer's influence on visual vortex structures from the draft tube's wall. Moreover, the local hydraulic loss distribution was clarified by using entropy production. By comparing Liutex magnitude distribution and entropy production rate, the vortex rope behavior effects on local hydraulic loss were significantly illuminated.

Key words: Cavitation; CFD; Entropy production; Francis turbine; Liutex method; vortex rope

1 INTRODUCTION

Francis turbines are the most popular in the generating capacity, and internal turbulence is highly complex. However, many Francis turbines are old and need renovation. Moreover, many studies have been done to redesign and renovate the runner to improve the cavitation characteristics. Among them, runners with splitter blades are considered the most promising way. Splitter blades can improve the load distribution on the runner blades, improve cavitation characteristics and decrease pressure pulsation compared with traditional runners [1]. The Francis-99 workshop series [2] looks to discuss and explore CFD techniques with application to Francis turbines with splitter blades. These studies proved to help a deeper understanding of the flow dynamics, mainly at transient operating and off-design conditions in a Francis-99 turbine. However, the internal vortex flows in the draft tube are complex; more studies are needed to demonstrate further Francis turbines' cavitating flow mechanism with splitter blades. Therefore, a rigorous capture of a vortex structure is indispensable for flow cavitation research.

The flow in the Francis turbine working at partial-load (PL) or high-load (HL) is unstable, leading to the development of the vortex rope. Various efforts have been performed to determine vortical structures in the Francis turbine. Tran et al. [3] used the Q - criterion to detect and analyze the vortex development at PL conditions. However, it is challenging to choose a threshold value and depends on the author's experience. Furthermore, by traditional vortex identification cannot be removed non-physical vortex structures. These will directly influence one's understanding of the hydraulic loss caused by vortex rope evolution. Recently, Liu et al. introduced the Ω method and Liutex/Rotex method [4] to determine the vortex. The Liutex/Rotex method has provided better performance and more reliability in revealing vortex structures [5, 6]. Hence, this method needs applying to analyze vortex rope's influence on the Francis turbine draft tube.

Usually, in a hydraulic turbine, hydraulic losses are determined by the difference in the total pressure of the inlet and the outlet. This method will not be able to illuminate the losses at any location's internal flow. Moreover, to overcome this, many works have been done

to prove the relationship between entropy production and hydraulic loss [7]. The entropy production theory [8] helps predict the turbine's hydraulic performance, so it is much simpler to get a quantitative locating address where energy dissipation occurs. However, they did not compare entropy production with vortex motion in a draft tube, which further clarifies the influence of vortex rope on hydraulic loss.

Motivated by the above literature, this paper aims to determine and illuminate better the cavitating vortex rope's influence on hydraulic loss. Hence, by the SST turbulence and ZGB cavitation models [9], the cavitation flow in the Francis-99 turbine is simulated. The cavitating vortex ropes in the draft tube of the Francis-99 turbine are captured. The vortex structure visualized by the Liutex/Rortex method is compared with the Ω method and Q - criterion. Furthermore, by comparing the distributions of entropy production rate, Liutex/Rortex and Ω method vortex rope's influence on hydraulic loss is further clarified.

2 MATHEMATICAL METHOD

The simulations are conducted based on the geometry and parameters provided by the second Francis-99 workshop. One of the crucial characteristics of the fluid flow problem in turbomachines is the runner rotational motion. Therefore, the rotating reference frame was used. Additionally, when simulating cavitating flow, the two phases are needed to be considered.

2.1 Governing Equations and Cavitation Model

In a rotating reference frame, the governing equation for absolute velocities can be expressed as follows:,

$$\frac{\partial \rho_m}{\partial t} + \frac{\partial (\rho_m u_i)}{\partial x_j} = 0 \tag{1}$$

$$\frac{\partial (\rho_m u_i)}{\partial t} + \frac{\partial (\rho_m u_i u_i^r)}{\partial x_j} = \frac{\partial p}{\partial x_j} + \frac{\partial}{\partial x_j}\left(\tau_{ij}^n + \tau_{ij}^t\right) - \rho \varepsilon_{ijk} \Omega_j u_k \tag{2}$$

$$\frac{\partial}{\partial t}(\alpha_v \rho_v) + \frac{\partial(\alpha_v \rho_v)}{\partial x_j} = R_e - R_c \tag{3}$$

where ρ_m - the mixture density; u_i - the absolute velocity components; u_i^r - the relative velocity components; p - the mixture pressure τ_{ij}^t - the turbulent stress tensor; τ_{ij}^n - the viscous stress tensor, ε_{ijk} - the Levi-Civita symbol; α_v, ρ_v - the volume fraction and density of vapor, respectively; R_e and R_c stand for evaporation and condensation during phase change.

Several mass transfer models can be used as the cavitation model, and it is presented to relate the single bubble radius R_B with the vapor volume fraction α_v. The ZGB cavitation model is adopted in the present study.

2.2 Vortex Identification Methods

The symmetric matrix and antisymmetric matrix of the velocity gradient tensor (∇V) are employed to identify the vortex.

$$\nabla V = \frac{1}{2}(\nabla V + \nabla V^T) + \frac{1}{2}(\nabla V - \nabla V^T) = \mathbf{A} + \mathbf{B} \tag{4}$$

a) Q - criterion
The Q- criterion can be written as: [10]

$$Q = \frac{1}{2}(b - a) \tag{5}$$

with:

$$a = \text{trace}(\mathbf{A}^T \mathbf{A}) = \sum_{i=1}^{3} \sum_{j=1}^{3} (A_{ij})^2 \tag{6}$$

$$b = \text{trace}(\mathbf{B}^T \mathbf{B}) = \sum_{i=1}^{3} \sum_{j=1}^{3} (B_{ij})^2 \tag{7}$$

And the zone with $Q \geq 0$ indicates the existence of the vortex. The Q criterion is widely used to identification vortex.

b) Ω method
Liu *et al.* [11] presented the Ω method as follows:

$$\Omega = \frac{b}{a + b + \varepsilon} \tag{8}$$

where a, b is defined the same as those in Eq. (5).

It is suggested that the vortex structures for most flows are most clearly identified when $\Omega = 0.52$. Therefore, the uniform value $\Omega = 0.52$ is used to visualize vortex structures on the Francis turbine in different operational points. However, Ω is adjusted in the range depending on the velocity flow.

c) Liutex/Rortex method
Unlike the above methods, the Liutex method shows both the magnitude R and direction $\vec{r}$ of the vortex as a vector [12]. The Liutex vector can be obtained by:

$$\vec{R} = R\vec{r} \tag{9}$$

$$R = \langle \vec{\omega}, \vec{r} \rangle - \sqrt{\langle \vec{\omega}, \vec{r} \rangle^2 - 4\lambda_{ci}^2} \tag{10}$$

$$\vec{R} = \left\{ \langle \vec{\omega}, \vec{r} \rangle - \sqrt{\langle \vec{\omega}, \vec{r} \rangle^2 - 4\lambda_{ci}^2} \right\} \vec{r} \tag{11}$$

2.3 Entropy Production Theory

Entropy production is an excellent variable for evaluating hydraulic loss and can be calculated by Eq. (13):

$$\dot{S}'''_D = \frac{\dot{Q}}{T} \tag{12}$$

For turbulent flows, $\dot{S}'''_D$ can be separated into two terms as:

$$\dot{S}'''_D = \dot{S}'''_{\overline{D}} + \dot{S}'''_{D'} \tag{13}$$

where $\dot{Q}$ stands for the energy transfer rate; $\dot{S}'''_{\overline{D}}$ and $\dot{S}'''_{D'}$ are specific entropy production rate, and can be defined as follows:

$$\dot{S}'''_{\overline{D}} = 2\frac{\mu_{eff}}{T}\left[\left(\frac{\partial \overline{u}}{\partial x}\right)^2 + \left(\frac{\partial \overline{v}}{\partial y}\right)^2 + \left(\frac{\partial \overline{w}}{\partial z}\right)^2\right] +$$
$$+ \frac{\mu_{eff}}{T}\left[\left(\frac{\partial \overline{u}}{\partial y} + \frac{\partial \overline{v}}{\partial x}\right)^2 + \left(\frac{\partial \overline{u}}{\partial z} + \frac{\partial \overline{w}}{\partial x}\right)^2 + \left(\frac{\partial \overline{v}}{\partial z} + \frac{\partial \overline{w}}{\partial y}\right)^2\right] \tag{14}$$

$$\dot{S}'''_{D'} = 2\frac{\mu_{eff}}{T}\left[\left(\frac{\partial u'}{\partial x}\right)^2 + \left(\frac{\partial v'}{\partial y}\right)^2 + \left(\frac{\partial w'}{\partial z}\right)^2\right] +$$
$$+ \frac{\mu_{eff}}{T}\left[\left(\frac{\partial u'}{\partial y} + \frac{\partial v'}{\partial x}\right)^2 + \left(\frac{\partial u'}{\partial z} + \frac{\partial w'}{\partial x}\right)^2 + \left(\frac{\partial v'}{\partial z} + \frac{\partial w'}{\partial y}\right)^2\right] \tag{15}$$

where $\overline{u}$, $\overline{v}$ and $\overline{w}$ are time-averaged velocity components; u', v' and w' cause by velocity fluctuation components.

However, when the results of simulations are obtained through the RANS approach, $\dot{S}'''_{\overline{D}}$ can be immediately determined, $\dot{S}'''_{D'}$ is not obtainable. According to Kock [13], for this, $\dot{S}'''_{D'}$ can be approximately calculated by:

$$\dot{S}'''_{D'} = \beta \frac{\rho \omega k}{T} \tag{16}$$

where k is the kinetic energy of the turbulent fluctuations.
Therefore, the local entropy production has been obtained after the numerical simulation. The overall

entropy production rate is the volume integration of the specific entropy production rate and can be obtained by:

$$S_{pro} = \int_v \dot{S}''_D \, dV \qquad (17)$$

2.4 Numerical Setup

This study used the Francis-99 model turbine as the study object. The main flow passage components of the Francis turbine are shown in Fig. 1. The Francis-99 workshop provided the grids on the corresponding flow zones. According to Trivedi et al. [14] the quality of these meshes satisfied the common industrial standard.

Table 1 Grid independence investigation [14]

Schemes	Grid number / 10^6	Efficiency η / %	Discrepancy / %
1	4.83	96.89	4.5
2	10.94	95.44	3.05
3	20.73	94.46	2.07

In this paper, the hydraulic efficiencies are chosen to evaluate the grid size's effect on the simulation results. As shown in Tab. 1, further increasing the grid number does not affect the calculation result. Grid scheme 3 (20.73 million nodes) is used for the numerical calculations.

The flow in hydro turbines is unsteady. Thus, unsteady simulations with one of the advanced turbulence models are necessary to predict the processing vortex rope. Moreover, in this case, the cavitating phenomenon could not be avoided. Therefore, the SST turbulence model was considered an appropriate model for predicting the vortex rope. Therefore, the SST turbulence model and ZGB cavitation model are approved in this study.

The boundary condition of the mass flow inlet was defined at the spiral casing inlet. The static pressure calculated from the cavitation coefficient (σ) is specified at the outlet of the draft tube. The zones between the runner and the guide blade/draft tube zone (interface) were used for the frozen rotor for steady-state. Also, for unsteady simulation, the transient rotor-stator condition was set. The runner rotational frequency for the present study was set at 5.54 Hz. The transient simulation time step corresponded to one degree of runner revolution ($t = 5 \cdot 10^{-4}$ s), and the value 10^{-5} was the maximum of convergence criterion.
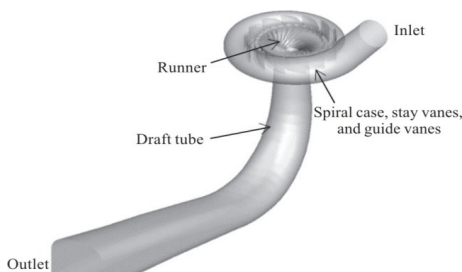

Figure 1 Francis-99 turbine

3 RESULTS AND ANALYSES
3.1 Validation of CFD Results

This paper used the data experiment provided by NTNU under the Francis-99 workshop series [2]. The axial velocities were presented with laser Doppler anemometry

(LDA) measurements along two horizontal planes in the draft tube [15]. We consider the two planes, Plane 1 and Plane 2 are located at lines L1 and L2 (see Fig. 2), respectively, along which we obtain the instantaneous velocity. In Fig. 3, for BEP condition operation, instantaneous velocity values and laser Doppler anemometry measurements data on Plane 1 and 2 corresponding Line 1 and Line 2 are normalized to be compared. As a result, there is an agreement between the experimental and numerical results.
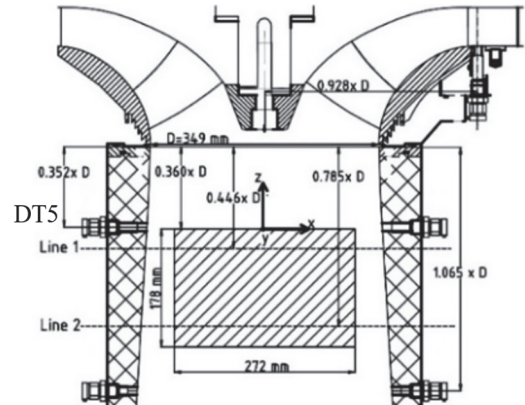

Figure 2 Positions of the experimental measurement lines 1 and 2 [2]
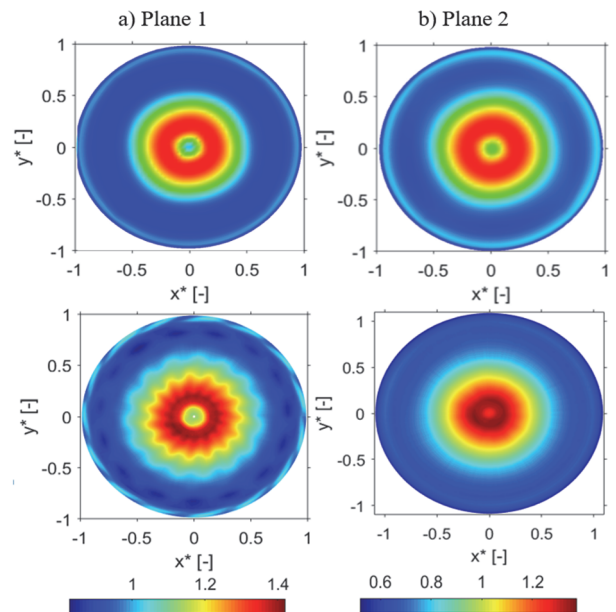

Figure 3 Vertical velocity at Plane 1 and Plane 2, comparison of numerical (above) and experimental (below)

Usually, the development of vortices is often related to fluctuations in pressure. Fig. 4 shows the frequency spectrum obtained by performed FFT analysis of the monitoring dynamic pressure fluctuation on the DT5 point (see Fig. 2) for PL condition. The figure shows a peak value of about 0.29 times the runner frequency, indicating vortex rope [16]. Fig. 4 also shows a second peak value at a lower frequency f_0 (about $0.1 \cdot f_{runner}$). This phenomenon suggests that the vapor volume in the draft tube cone causes a significant drop in the wave speed. The pressure fluctuations are significantly amplified in the resonance case, which can put the hydro-mechanical system's stability in the harmful case.
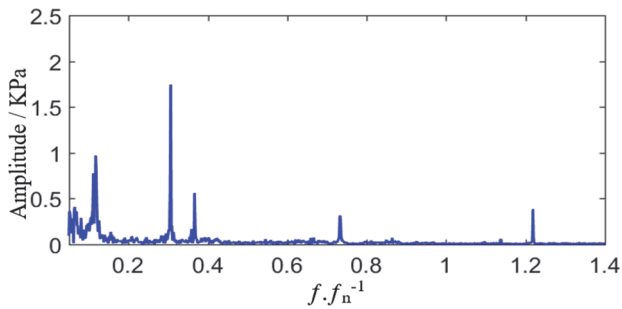
Figure 4 Pressure fluctuation frequency at DT5 point for the PL condition

From the above comparisons, the simulation results are in good agreement with the experimental data. Therefore

3.2 Spiral Vortex Breakdown Visualized by Ω Method and Liutex/Rortex Method

Cavitation and vortex interact in the flow field; thus, a rigorous capture of a vortex structure is essential for flow cavitation investigation. This section identifies and investigates vortex structures in the Francis-99 turbine draft tube operating under PL conditions.

Fig. 5 shows the comparison of the iso-surfaces given by the Q - criterion, Ω method, and Liutex/Rortex method. The pictures reveal no graphical differences between the results of the Ω method and Q - criterion for visualization vortex rope, where the chosen Q - criterion values are optimized. The method, which $\Omega = 0.52$, could successfully capture the vortex structure that misses the subjective adjustment of the threshold values. However, when using the Q - criterion and method, some non-vortical structures (see Fig. 5b) are still observed, caused by the draft tube's boundary layer. In particular, the Q - criterion does not capture the vortex structures when a high threshold is used.

In contrast, in the Liutex/Rortex method in Fig. 5c, the unique vortex rope is observed more clearly. Furthermore, the Liutex method can effectively remove the boundary layer's influence of the draft tube's wall on visual vortex structures. Thus, for multi-phase flows, the Liutex/Rortex method works better than the method and Q - criterion.
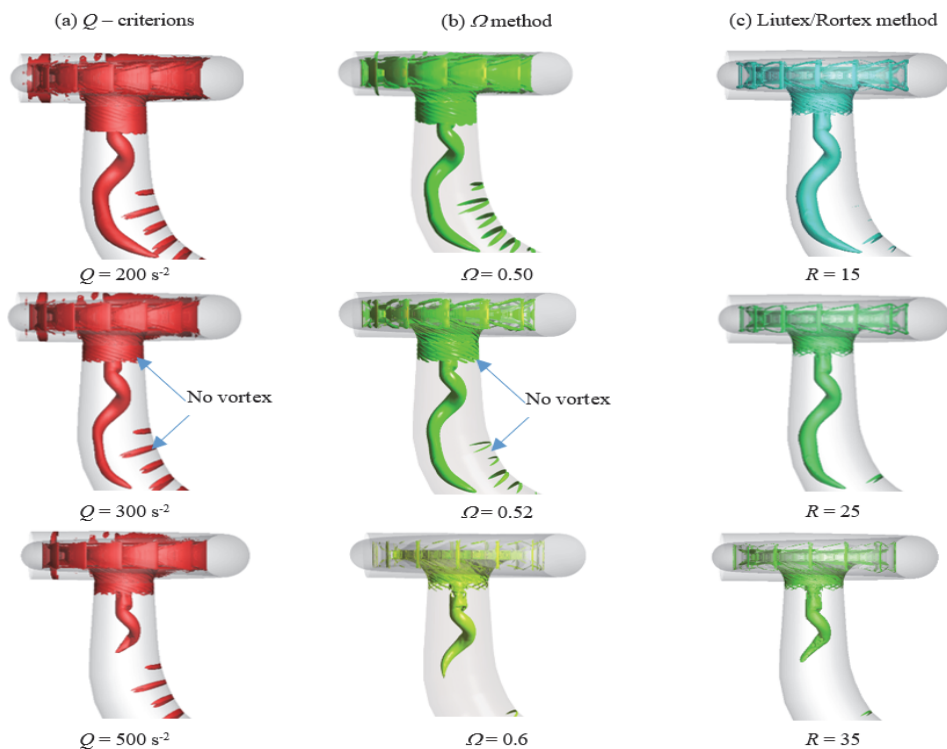

Figure 5 Comparisons for the vortex identification between the Q - criterion (a), Ω method (b), and Liutex/Rortex (c) iso-surfaces
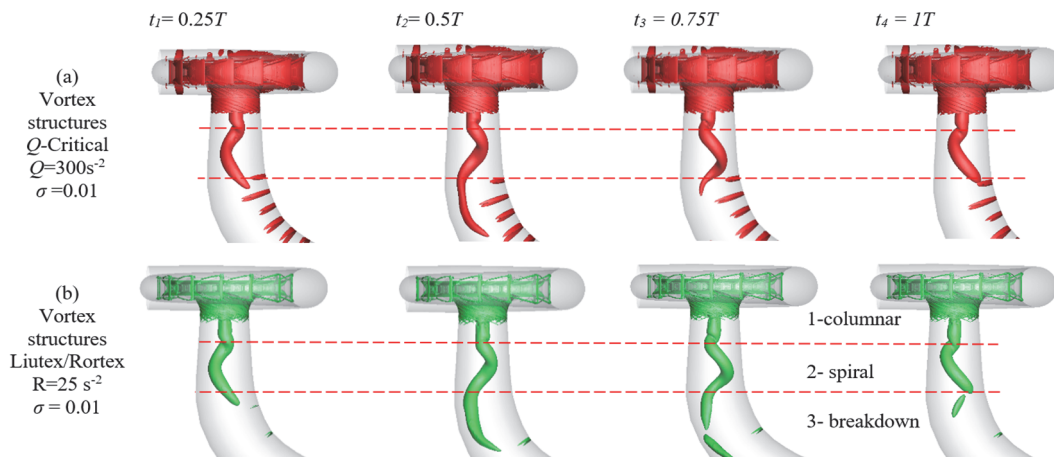

Figure 6 Vortex structures evolution in one cycle for two critical cavitation conditions at PL operating point

To further understand the turbulent flow characteristics in the draft tube, the visualization vortex evolutions using Liutex/Rortex method and Q - criterion based on the unsteady simulation are employed and compared. Fig. 6 shows the evolution of vortex structure in a revolution period under critical cavitation conditions. The vortex rope is divided into three axial sub-regions. In Region 1 (near the runner outlet regime), a nearly straight vortex rope is observed. Region 2 consists of a spiral rope, which rotates and translates with predetermined velocities. Region 3 shows vortex breakdown, shedding, and moves downstream. The cavitation is strongly developed within the first region, and its precession motion almost looks like a symmetrical axis. Within region 3, the diameter near the tail of the vortex rope decreases. The vortex rope precession loses its coherence, and the volume of the vortex rope changes a lot in one rotation period due to the vortex breakdown. As shown in Fig. 6, the vortex strength represented by the Q - criterion has significantly been diminished at the downstream (region 3), which is discrepant from the results shown by the Liutex/Rortex method. Furthermore, it can be seen that the process of vortex breakdown occurs rapidly but is only well captured by Liutex/Rortex method without any vortices cloud.
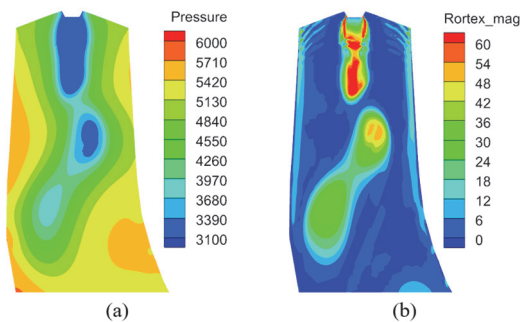

Figure 7 Distribution of instantaneous pressure (a) and instantaneous Liutex/Rortex (b)

Fig. 7 shows the comparison of the Liutex/Rortex distribution's relative locations with the pressure. Fig. 7a the low-pressure zones represent cross-sections of the spiral vortex rope due to the balance of centripetal force in the vorticity axis [17]. The figure shows that the distribution of the instantaneous pressure and Liutex/Rortex is similar. These results are further confirmation of the genuineness of the Liutex method.

4 INFLUENCE OF VORTEX ROPE ON ENERGY LOSS

In hydraulic machinery, the hydraulic efficiency of the turbine usually can be calculated as:

$$\eta = \frac{M \cdot \omega}{\rho g H Q} \tag{18}$$

where H is the head calculated by $(p_1 - p_2)/\rho g$ and p_1 and p_2 represent total pressure at the turbine inlet and outlet.

Fig. 8 compares the hydraulic efficiency calculated by entropy production and the method of the total pressure drop. It can be seen that both curves of the hydraulic performances calculated using entropy production and the pressure drop are in agreement. At lower flow conditions,

the flow in the turbine occurs with strong vortex rope and cavitation. High entropy production rate focuses where the cavitating vortex rope occurs. The loss of energy determined through entropy included the vortex behavior and effect of the boundary layer. Therefore, there is a deviation between the results of both methods at the low flow condition, hence further confirmations of the close relationship between entropy production and hydraulic loss.
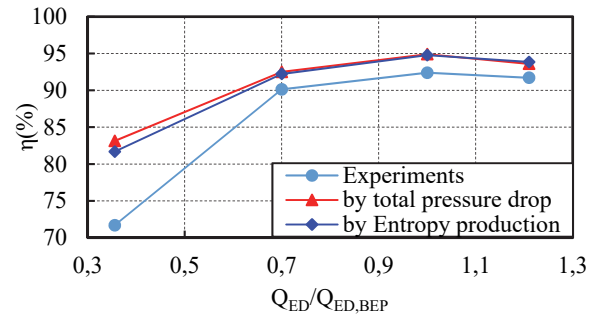

Figure 8 Efficiency calculated by simulations and experiment
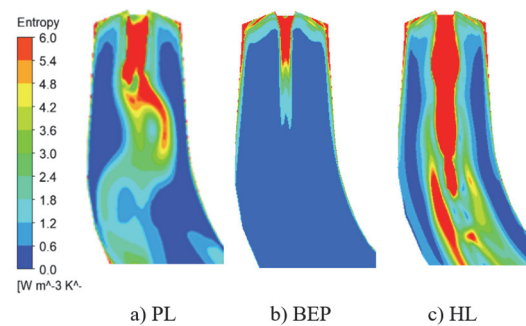

a) PL b) BEP c) HL
Figure 9 Distribution of entropy production on the meridian plane of the draft tube

The draft tube is designed to reduce the exit velocity of flow; thus, recovery pressure decreases the exit loss and improves efficiency. However, it has been shown that effective pressure recovery is prevented according to the flow conditions. It is assumed that the significant development of a dead water region preventing the main flow in the draft tube cone causes significantly high specific energy losses. Fig. 9 shows the entropy production distribution on the draft tube's meridian plane for three operating conditions. The pictures indicate the significant dissipation in the draft tube. The high entropy production region occurs at off-design operating conditions (Fig. 9a and Fig. 9c), which shows that hydraulics losses are higher at these conditions. The entropy production in the draft tube is remarkably high, which indicates that the specific energy loss in the draft tube is exceptionally high.

As discussed above, under off-design operating appears vortex rope in the draft tube. Therefore, to clarify the vortex rope's influence on hydraulic loss further, the entropy production is compared with vortex motion in a Francis turbine draft tube. Fig. 10 compares the high entropy production region in the draft tube, and the high entropy region rotates with the vortex rope motion at several time steps. The area with high entropy production appears in the draft tube. Moreover, it turns with the vortex rope and contains the vortex rope center but has a more extensive range. The presented results suggest that the high entropy production regime covers the vortex structure. The evolution of a vortex rope at the centerline of the draft tube

is responsible for the development entropy production rate. Also, the formation of the vortex rope can be predicted well by analysis of entropy production.
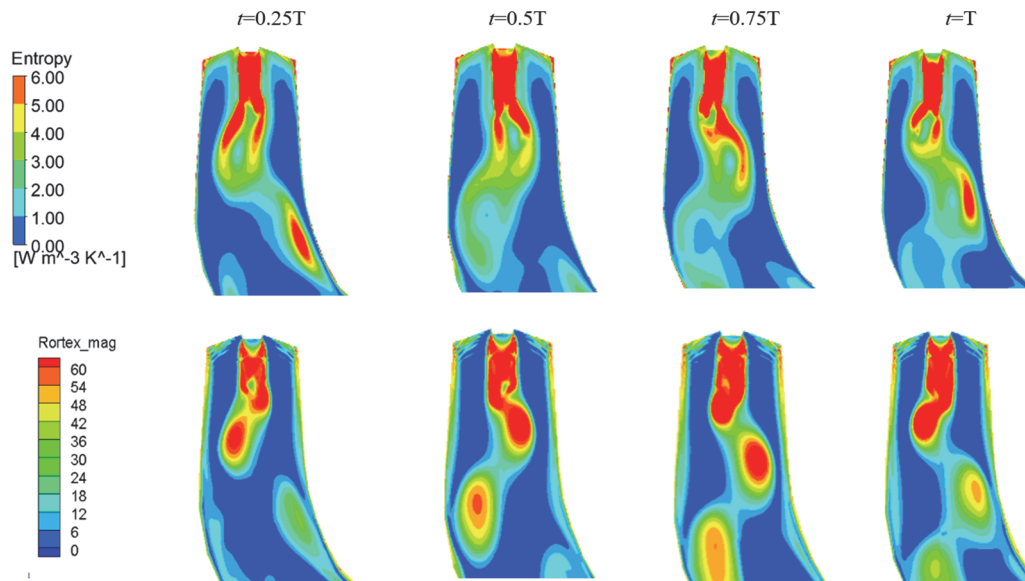

Figure 10 Contours of (a) instantaneous distribution of entropy production, (b) instantaneous Liutex/Rortex on the meridian plane of the draft tube at PL

Fig. 10 also shows that the vortex ropes' processing affects the generated entropy production. It indicates that the vortex rope had the same evolution cycle with entropy production rate. Therefore, the behavior of evolution vortex rope in the draft tube significantly affects the local Liutex magnitude distribution. As a result, it increases the local entropy generation rate causing the local hydraulic loss. It shows that the vortex rope induced unsteady flow and increased the hydraulic loss.

5 CONCLUSIONS

For the identifications of the vortex rope structure, the W method has more advantages than other current methods (e.g., Q - criterion) and can avoid subjective errors in threshold value selection. However, the Liutex method can effectively remove the boundary layer's influence on visual vortex structures from the draft tube's wall.

By comparing entropy production with the evolution of cavitating vortex rope, the study of entropy production can predict the development of the vortex rope. Furthermore, the agreement of vortex and local entropy production rate was illustrated. The influence of the vortex rope on local hydraulic loss was addressed.

6 REFERENCES

[1] Hou, Y., Li, R., & Zhang, J. (2012). Research on the Length Ratio of Splitter Blades for Ultra-high Head Francis Runners. *Procedia Engineering*, 31, 92-6. https://doi.org/10.1016/j.proeng.2012.01.996

[2] Francis-99 Workshop 2: transient operation of Francis turbines. *Journal of Physics: Conference Series.* 2017; 782:11001. https://doi.org/10.1088/1742-6596/782/1/011001

[3] Tran, C., Bin, J., & Long, X. (2019). Simulation and Analysis of Cavitating Flow in the Draft Tube of the Francis Turbine with Splitter Blades at Off-Design Condition. *Tehnicki vjesnik - Technical Gazette*, 26, 1650-1657. https://doi.org/10.17559/TV-20190316042929

[4] Xu, H., Cai, X., & Liu, C. (2019). Liutex (vortex) core definition and automatic identification for turbulence vortex structures. *Journal of Hydrodynamics*, 31, 857-63. https://doi.org/10.1007/s42241-019-0066-5

[5] Yu, Y., Shrestha, P., Alvarez, O., Nottage, & C., Liu, C. (2020). Correlation analysis among vorticity, Q method and Liutex. *Journal of Hydrodynamics, 32*, 1207-11. https://doi.org/10.1007/s42241-020-0069-2

[6] Tran, C. T., Long, X., Ji, B., & Liu, C. (2020). Prediction of the precessing vortex core in the Francis-99 draft tube under off-design conditions by using Liutex/Rortex method. *Journal of Hydrodynamics*, 32, 623-8. https://doi.org/10.1007/s42241-020-0031-3

[7] Herwig, H. & Schmandt, B. (2014). How to Determine Losses in a Flow Field: A Paradigm Shift towards the Second Law Analysis. *Entropy*, 16, 2959-89. https://doi.org/10.3390/e16062959

[8] Bejan, A. & Kestin, J. (1983). Entropy Generation Through Heat and Fluid Flow. *Journal of Applied Mechanics, 50*, 475. https://doi.org/10.1115/1.3167072

[9] Zwart, P., Gerber, A., & Belamri, T. (2004). A two-phase flow model for predict ing cavitation dynamics. *In: Fifth International Conference on Multiphase Flow,* Yokohama, Japan, 152.

[10] Hunt, J., Wary, A., & Moin, P. (1988). *Eddies, streams, convergence zones in turbulent flows Proceedings of the Summer Program 1988 in its Studying Turbulence Using Numerical Simulation Databases*. Stanford, California, USA, 193-208.

[11] Liu, C., Wang, Y., Yang, Y. et al. (2016). New omega vortex identification method. *Science China Physics Mechanics and Astronomy*, 59(8), 1-9. https://doi.org/10.1007/s11433-016-0022-6

[12] Shrestha, P., Nottage, C., Yu, Y., Alvarez, O., & Liu, C. (2021). Stretching and shearing contamination analysis for Liutex and other vortex identification methods. *Advances in Aerodynamics, 3*, 8. https://doi.org/10.21203/rs.3.rs-86116/v1

[13] Kock, F. & Herwig, H. (2004). Local entropy production in turbulent shear flows: a high-Reynolds number model with wall functions. *International Journal of Heat and Mass Transfer*, *47*, 2205-15. https://doi.org/10.1016/j.ijheatmasstransfer.2003.11.025

[14] Trivedi, C., Cervantes, M. J., Gandhi, B. K., & Dahlhaug, O. G. (2013). Experimental and numerical studies for a high head francis turbine at several operating points. *Journal of Fluids Engineering*, *135*(11), 111102. https://doi.org/10.1115/1.4024805

[15] Sundstrom, L. R. J., Amiri, K., Bergan, C., Cervantes, M. J., & Dahlhaug, O. G. (2014). LDA measurements in the Francis-99 draft tube cone. *IOP Conference Series: Earth and Environmental Science*, *22*, 22012. https://doi.org/10.1088/1755-1315/22/2/022012

[16] Nishi, M. & Liu, S. (2013). An Outlook on the Draft-Tube-Surge Study. *International Journal of Fluid Machinery and Systems*, *6*, 33-48. https://doi.org/10.5293/IJFMS.2013.6.1.033

[17] Favrel, A., Müller, A., Landry, C., Yamamoto, K., & Avellan, F. (2015). Study of the vortex-induced pressure excitation source in a Francis turbine draft tube by particle image velocimetry. *Experiments in Fluids, 56*(12), 215-230. https://doi.org/10.1007/s00348-015-2085-5

Contact information

Cong Trieu TRAN
(Corresponding Author)
Hydraulic Engineering department, Hanoi University of Civil Engineering - 55
Giai Phong, Hanoi, Vietnam
E-mail: trancongtrieu@whu.edu.cn

Duc Cuong PHAM
Hydraulic Engineering department, Hanoi University of Civil Engineering - 55
Giai Phong, Hanoi, Vietnam
Email: cuongpd@nuce.edu.vn